

Observation of a Charge-2 Photonic Weyl Point in the InfraredSachin Vaidya¹, Jiho Noh¹, Alexander Cerjan¹, Christina Jörg^{1,2},
Georg von Freymann^{2,3} and Mikael C. Rechtsman^{1,*}¹*Department of Physics, The Pennsylvania State University, University Park, Pennsylvania 16802, USA*²*Physics Department and Research Center OPTIMAS, Technische Universität Kaiserslautern, 67663 Kaiserslautern, Germany*³*Fraunhofer Institute for Industrial Mathematics ITWM, 67663 Kaiserslautern, Germany*

(Received 18 March 2020; revised 27 October 2020; accepted 9 November 2020; published 17 December 2020)

Weyl points are robust point degeneracies in the band structure of a periodic material, which act as monopoles of Berry curvature. They have been at the forefront of research in three-dimensional topological materials as they are associated with novel behavior both in the bulk and on the surface. Here, we present the experimental observation of a charge-2 photonic Weyl point in a low-index-contrast photonic crystal fabricated by two-photon polymerization. The reflection spectrum obtained via Fourier-transform infrared spectroscopy closely matches simulations and shows two bands with quadratic dispersion around a point degeneracy.

DOI: [10.1103/PhysRevLett.125.253902](https://doi.org/10.1103/PhysRevLett.125.253902)

Over the past decade, topological materials have been studied extensively in the hopes of harnessing properties such as protection from defects and scatter-free transport. The simplest topological systems in three dimensions are Weyl materials, which possess a set of point degeneracies in momentum space that act as sources of Berry curvature [1], and are thus topologically protected against perturbations to the system. In this sense, Weyl points are analogous to magnetic monopoles in momentum space and are associated with a quantized topological charge. A direct consequence of their nonzero charge is that perturbations that preserve periodicity cannot cause a gap to open at the Weyl point but merely displace it in the band structure. Moreover, these materials exhibit unusual surface states that lie on Fermi arcs connecting Weyl points of opposite charges. The necessary conditions for the existence of Weyl points are very general and only require breaking either inversion symmetry, time-reversal symmetry, or both. Since these conditions can be met in a wide range of physical systems, Weyl points have been shown to exist in solids [2–9], microwave [10,11] and optical photonic crystals (PhC) [12], optical waveguide arrays [13,14], circuit-based systems [15], mechanical crystals [16], phononic crystals [17,18], metamaterials [19], magnetized plasmas [20], and in systems with synthetic dimensions [21].

If a Weyl material has additional spatial symmetries, it is possible for multiple Weyl points of the same charge and between the same two bands to accumulate at high symmetry points in the Brillouin zone leading to Weyl points with a higher topological charge [22,23]. For example, a parity-breaking chiral woodpile PhC made of stacked layers of dielectric rods ($n = 3.4$) has been predicted to have charge-2 Weyl points [24] that form due to the presence of a screw symmetry. This symmetry pins the

location of the ± 2 charges to high symmetry points in the Brillouin zone of the PhC [23], which implies that as long as the required spatial symmetries are present, these charge-2 Weyl points must continue to exist regardless of index contrast. While other studies report findings of higher-charged Weyl points, their implementations are limited to macroscopic metallic PhCs that work in microwave frequencies [25] and acoustic structures [26].

In this Letter, we report the experimental observation of a charge +2 Weyl point in the mid-infrared regime in a low-index ($n = 1.52$) chiral woodpile PhC fabricated by two-photon polymerization and characterized using angle-resolved Fourier-transform infrared (FTIR) spectroscopy. For such a low index contrast, there is only an incomplete band gap surrounding the Weyl point. Nevertheless, we show that this is sufficient to directly observe the dispersion features associated with the Weyl point in the reflection spectrum of the PhC. Furthermore, we numerically show the existence of topological surface resonances, akin to Fermi arc states, associated with Weyl points that satisfy the bulk-boundary correspondence in the absence of a band gap. The prospect of lowering the index contrast requirements for achieving topological photonic structures is of importance since it can allow for readily available fabrication techniques to be used. This includes methods such as colloidal and polymer self-assembly and the two-photon polymerization process, both of which commonly employ low-index materials.

The specific PhC we use to realize a charge +2 Weyl point is a chiral woodpile as shown in Fig. 1(a), whose 3D unit cell consists of four layers of rectangular rods stacked on top of each other with a relative 45° in-plane rotation. The width and height of the rods is $0.175a$ and $0.25a$, respectively, where a is the lattice constant in all three

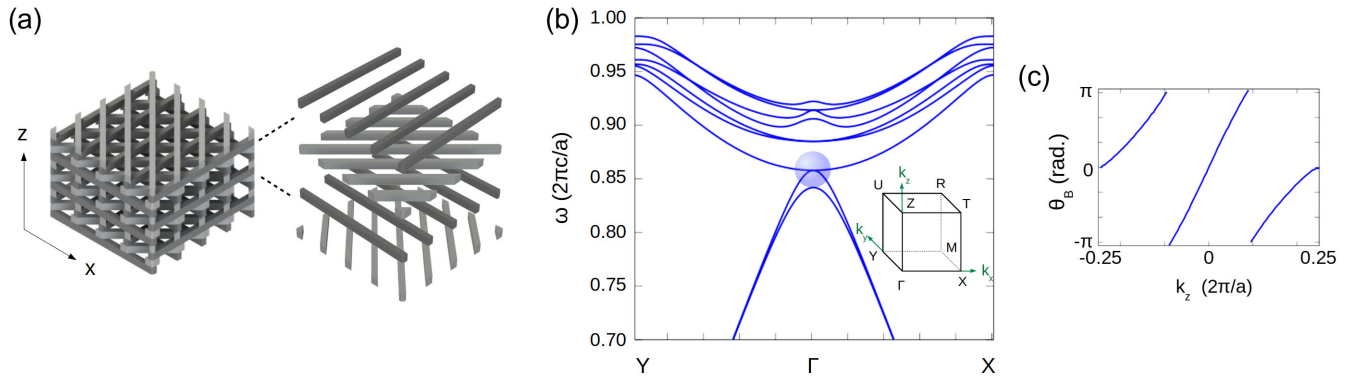


FIG. 1. Chiral woodpile PhC and corresponding band structure supporting a charge +2 Weyl point. (a) The chiral woodpile structure made by stacking layers of rods with an in-plane rotation of 45° between layers. (b) Band structure along $\mathbf{Y} - \Gamma - \mathbf{X}$ showing bands 3 to 11. The Weyl point of interest is the degeneracy between bands 4 and 5 at Γ (blue circle). The 3D Brillouin zone of the PhC is shown in the inset. (c) Berry phase plot for band 4 around the Γ point. The double winding indicates that the degeneracy has a topological charge of 2.

directions. The spacing between the rods in the 45° and 135° layers is $a/\sqrt{2}$. The rods have a dielectric constant (ϵ_{rods}) of 2.31, which corresponds to the material used in the experiment [27]. Using these parameters, the band structure of our PhC is numerically calculated using MPB [28], and bands 3 to 11 along $\mathbf{Y} - \Gamma - \mathbf{X}$ are shown in Fig. 1(b). The degeneracy at Γ between bands 4 and 5 is the Weyl point of interest. These bands along $\Gamma - \mathbf{Z}$ direction in the Brillouin zone are very close in frequency but convergence tests show that the degeneracy only occurs at the Γ point. To confirm the topological nature of this degeneracy, we directly calculate its topological charge (Chern number) by using a discrete algorithm to compute Berry phase (θ_B) given in Ref. [29]. The phase is directly calculated using magnetic field eigenmodes from MPB on contours that are defined by constant k_z and enclose the Weyl point. The topological charge of the Weyl point is equal to the number of times θ_B winds around as a function of k_z as shown in Fig. 1(c). (See Supplemental Material [30] for full band structure and details on Berry phase calculation). A second Weyl point of charge -2 between the same two bands is located at the \mathbf{R} point in the Brillouin zone, which exhibits double winding of Berry phase in the opposite sense. Since this Weyl point is located below the light line of air and as such is inaccessible without the use of gratings or high-index fluids, we choose to measure the Weyl point at Γ in our experiment.

For the experiment, we fabricate the chiral woodpile PhC by 3D lithography (direct laser writing, DLW [31]) using a DLW instrument (Photonic Professional GT, Nanoscribe GmbH), which employs two-photon polymerization of a liquid negative tone photoresist (IP-DIP, Nanoscribe GmbH) ($n = 1.52$). Here, we use DLW in dip-in configuration [32], where the microscope objective (63x, NA = 1.4) for DLW is dipped into the photoresist applied below the fused-silica substrate. The 3D structure is then

written layer by layer starting from the bottom surface of the substrate by moving the microscope objective in the z direction. The structure is developed in propylene glycol monomethyl ether acetate (PGMEA) for 20 min and then developed in isopropanol for 3 min. The thickness of the rods is controlled by varying the number of superpositions of individual laser writing for each rod [33]. The sample has a lattice constant of $4 \mu\text{m}$ and rod width and height equal to 700 nm and $1 \mu\text{m}$, respectively. We fabricate 20 unit cells in the z direction (80 layers) and 250 unit cells in the x and y directions. An image of one such sample taken by field emission scanning electron microscopy (FESEM) is shown in Fig. 2.

Reflection measurements are carried out using the Bruker Vertex 80 FTIR spectrometer at wavelengths ranging from $4.2\text{--}6 \mu\text{m}$ with the frequency resolution set to 8 cm^{-1} . A variable angle reflection accessory (Seagull) is used to observe the angle-resolved spectra from 0° to 15° along the $\Gamma - \mathbf{X}$ direction with a resolution of 1° . The data for -15° to 0° is identical to the data for the corresponding positive angles since the structure is invariant under 180° rotational symmetry about the z axis and hence we only measure data for positive angle and reflect it for negative angles. A polarizer is used at the output port to obtain spectra for 0° (s), 45° , and 90° (p) polarizations. The spectrum is normalized to the maximum value of reflection for each angle and interpolated. The results from the experiment are shown in Figs. 3(a), 3(b), and 3(c). We also numerically simulate the reflection spectrum using rigorous coupled-wave analysis (RCWA) as implemented in S^4 [34] where periodic boundary conditions are imposed in the lateral directions and the structure is finite in the z direction having 20 unit cells. The simulation results are shown in Figs. 3(d), 3(e), and 3(f) for comparison. As can be seen, the simulated and experimentally measured spectra match very well and show sharp quadratic boundaries

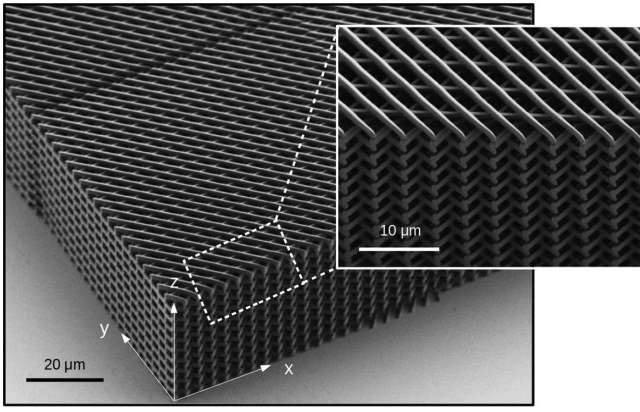


FIG. 2. Fabricated chiral woodpile PhC. FESEM image of a parity-breaking chiral woodpile fabricated using two-photon polymerization.

separating reflective and transmissive regions that match each of the two relevant bulk Weyl bands in orthogonal polarizations. As expected, the measurement for 45° polarization is a superposition of measurements for s and p polarizations and shows clear signatures from both bands forming the Weyl point at the degeneracy. To provide further support for the robustness of our Weyl point, we also fabricate and measure a chiral woodpile PhC with significantly different dimensions but with preserved screw symmetry and observe the same Weyl point (see Supplemental Material [30]). In this case, the lattice constant of the PhC is $2.1 \mu\text{m}$, which puts the Weyl point

at a near-IR wavelength of $2.4 \mu\text{m}$. This additional measurement also represents a large step forward towards bringing Weyl points in PhCs down to telecommunication and visible wavelengths.

Since the PhC investigated here has low index contrast, there is no complete band gap around the Weyl point, and therefore this relatively unobscured direct observation warrants further explanation. When probing reflection through the chiral woodpile, we make the assumption that the sample is effectively infinite in the x and y directions (parallel to the surface) and truncated in the z direction; we thus examine the projected band structure, since k_z is no longer conserved (but k_x and k_y still are). As such, the projected band structure consists of states with both $k_z = 0$ and $k_z \neq 0$ projected onto the (k_x, k_y) plane. Thus, even though the Weyl point exists in an incomplete band gap in the 3D Brillouin zone of our chiral woodpile PhC, in the projected band structure there are states from other bands which are now degenerate with the Weyl point in frequency and with the same k_x and k_y , and one may expect that these overlapping states would obscure the signature of the Weyl point in the reflection spectrum. However, the agreement we observe between the 3D band structure calculations [Fig. 1(b) and dashed lines in Fig. 3] and the reflection spectrum (Fig. 3) suggests that this measurement is relatively insensitive to these overlapping states. To further explore this feature in our results, we calculate the modal overlaps between s - and p -polarized plane waves and the Bloch modes of the PhC. Two parameters are defined using these modal overlaps that measure the polarization of the

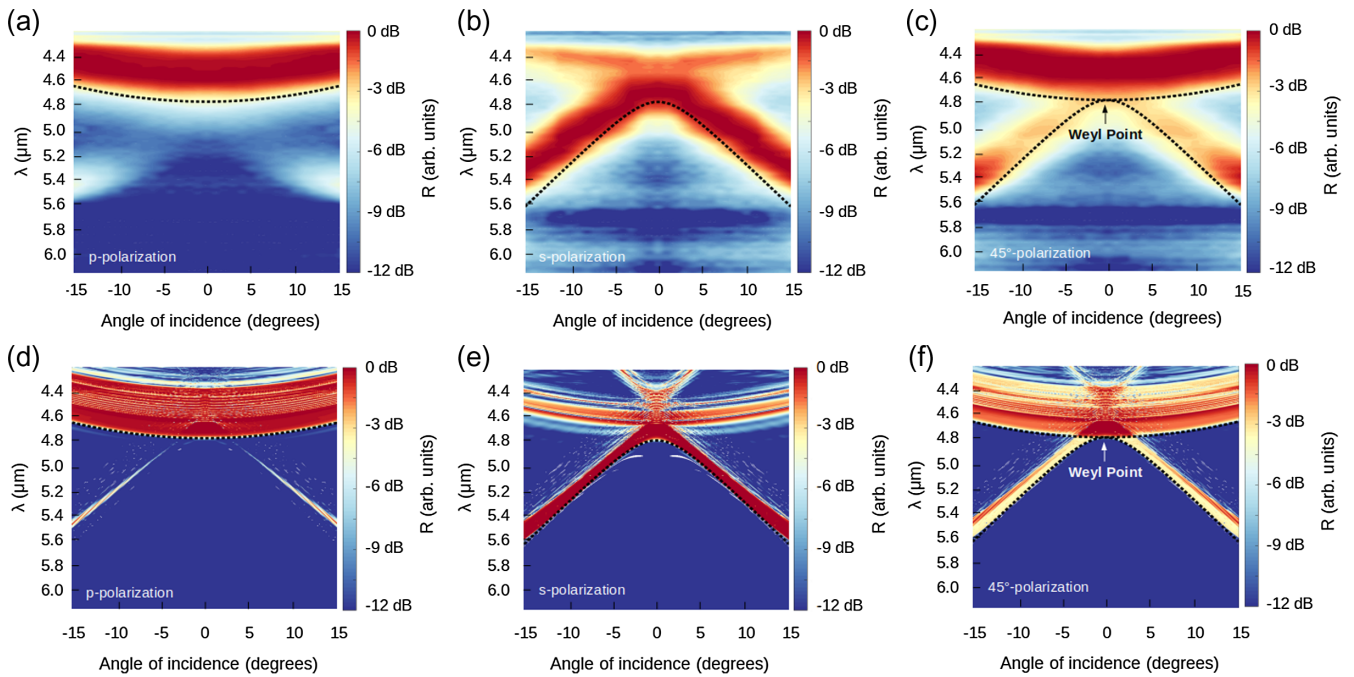


FIG. 3. Observation of the charge $+2$ Weyl point in the reflection spectra of the chiral woodpile PhC. (a),(b),(c) Experimentally measured angle-resolved FTIR reflection spectra for 90° (p), 0° (s) and 45° polarizations, respectively. The dotted lines in all plots are Weyl bulk bands from MPB. (d),(e),(f) S^4 (RCWA) simulation of the angle-resolved reflection spectra for all three polarizations.

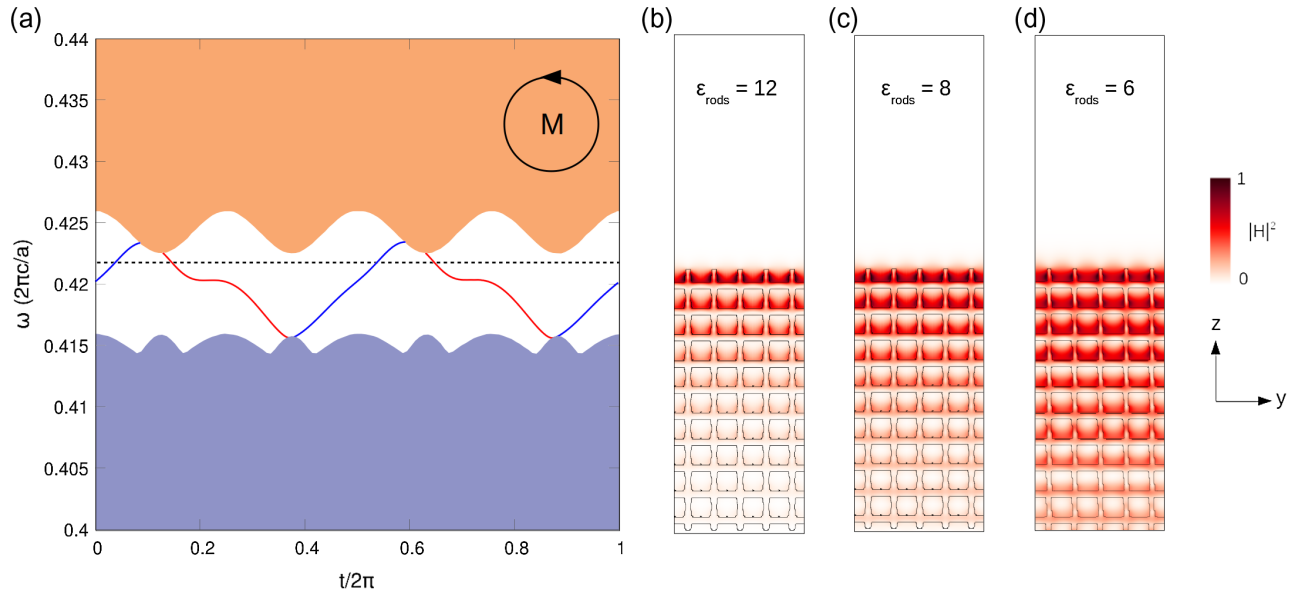


FIG. 4. Surface states associated with the Weyl point at \mathbf{R} (a) The k_z -projected band structure for the truncated chiral woodpile PhC ($\epsilon_{\text{rods}} = 12$, rod width = $0.175a$, rod height = $0.25a$) along a loop enclosing the \mathbf{M} point with radius $0.15 (2\pi/a)$ and parametric angle $0 \leq t/2\pi \leq 1$. Solid colors are projections of bulk bands, the solid red and blue lines are surface states localized to the top and bottom surfaces, respectively, and the black dotted line marks the frequency of the Weyl point. (b)–(c) Magnetic field intensity of the surface state at $t/2\pi = 0.25$ for $\epsilon_{\text{rods}} = 12$ and 8 , respectively. (d) Magnetic field intensity of the surface resonance for $\epsilon_{\text{rods}} = 6$ calculated using FDTD method as implemented in MEEP [40].

Bloch modes and the overall in-coupling of an arbitrarily polarized plane wave [35–38]. These parameters indicate that the modes with $k_z \neq 0$ in the projected band structure, which would have otherwise obscured the observation of the Weyl point, either have a polarization mismatch with the incident light and/or have inefficient mode in-coupling. This leads to the observed features in the reflection spectrum wherein the boundaries of highly reflecting regions correspond to the $k_z = 0$ Weyl bands (see Supplemental Material [30] for a detailed analysis). More generally, this kind of polarization analysis can be useful for any low-contrast PhCs where the projected band structure is insufficient to infer the origins of spectral features from the band structure.

The topological charge associated with Weyl points gives rise to surface states, analogous to Fermi arc states, which are a direct consequence of the bulk-boundary correspondence. However, at low dielectric contrast, as in the present experiment, the overlapping states and the lack of a band gap imply that any surface states associated with the Weyl points are leaky resonances that are degenerate with bulk eigenstates of the PhC. Even at high dielectric contrast, the surface states associated with the Weyl point at Γ are resonances for two reasons: (i) When the structure is truncated, surface states lie above the light line of air and confinement on this side requires a trivial band gap material and (ii) the dispersion of the bands for our structure does not allow the opening of a local band gap around the Weyl point. We have found that such resonances

(if present) are too broadened by leakage to be observable for the index contrast of the photonic crystal used here. However, both these issues are resolved when examining a high-contrast version of our PhC, in the vicinity of the charge -2 Weyl point at \mathbf{R} [$k_x = k_y = k_z = 0.5 (2\pi/a)$], which we consider for the following numerical analysis.

In a chiral woodpile PhC with $\epsilon_{\text{rods}} = 12$ and truncated in the z direction, we examine the surface band structure along a circular loop enclosing the projection of the Weyl point [26,39]. This loop has radius $0.15 (2\pi/a)$ and is parametrized by an angle $0 \leq t/2\pi \leq 1$. The surface band structure as plotted in Fig. 4(a) reveals the existence of Fermi arc surface states in the nontrivial gap formed along the loop. Because of the bulk-boundary correspondence, the number of these surface states that cross the bulk band gap is equal to the Chern number of the enclosed degeneracy, which in this case is -2 . The sign corresponds to the direction of motion of the surface states. The magnetic field intensity of the surface state localized to the top edge is plotted in Fig. 4(b), which shows strong confinement to the PhC-air interface. We repeat these calculations for progressively smaller values of dielectric contrast and find that a local gap fails to open at $\epsilon_{\text{rods}} \sim 6$ around the loop considered here and at $\epsilon_{\text{rods}} \sim 5$, a local gap fails to open for a loop of any radius. Examining the field intensity profile from a finite-difference time-domain (FDTD) simulation [40], shown in Fig. 4(d), reveals that at $\epsilon_{\text{rods}} = 6$, the surface state is now a leaky resonance with a Q factor $\sim 10^3$. As we can see, the confinement of the surface state relies on the

existence of at least a local band gap, which heavily depends on the dielectric contrast (see animated file in Supplemental Material [30]). For the dielectric contrast of our experiment, namely, $\epsilon_{\text{rods}} = 2.31$, the resonances have broadened sufficiently to be effectively unobservable. On the other hand, changing the dielectric contrast does not break the screw symmetry in our structure and as such does not affect the existence of the Weyl points, whether at the Γ or \mathbf{R} points. Therefore, although the surface states in our low-contrast PhC have turned into resonances that extend into the bulk, the charge ± 2 Weyl points have a continued existence due to their symmetry protection.

To summarize, we have presented the observation of a charge $+2$ Weyl point in a 3D PhC in the midinfrared regime. The fact that we have used a relatively low refractive index polymer demonstrates the possibility of exploring 3D topological phenomena in the IR and into optical frequencies, where very high-index, low-loss materials may not be available or amenable to 3D device fabrication. It will be of interest in the future to explore surface resonances in 3D PhCs with Weyl points; these will have fundamentally different properties compared to traditional surface states because of radiative loss, which will give rise to non-Hermitian effects on the surface.

M.C.R. acknowledges support from the ONR YIP program under Grant No. N00014-18-1-2595, the Packard Foundation (2017-66821), and the Penn State NSF-MRSEC Center for Nanoscale Science, under Grant No. DMR-1420620. J.N. acknowledges support by Corning Incorporated Office of STEM Graduate Research. C.J. gratefully acknowledges funding from the Alexander von Humboldt Foundation within the Feodor-Lynen Fellowship program. G.v.F. acknowledges support by the Deutsche Forschungsgemeinschaft through CRC/Transregio 185 OSCAR (project no. 277625399). We are grateful to Josh Stapleton and Tawanda J. Zimudzi for technical help with the FTIR spectrometer and Kathleen Gehoski for technical help with Nanoscribe. S.V. acknowledges Debadarshini Mishra for helpful discussions on the topic.

S. V. and J. N. contributed equally to this work.

*mcrworld@psu.edu

- [1] M. V. Berry, *Proc. R. Soc. A* **392**, 45 (1984).
- [2] S.-Y. Xu, I. Belopolski, N. Alidoust, M. Neupane, G. Bian, C. Zhang, R. Sankar, G. Chang, Z. Yuan, C.-C. Lee, S.-M. Huang, H. Zheng, J. Ma, D. S. Sanchez, B. Wang, A. Bansil, F. Chou, P. P. Shibayev, H. Lin, S. Jia, and M. Z. Hasan, *Science* **349**, 613 (2015).
- [3] X. Wan, A. M. Turner, A. Vishwanath, and S. Y. Savrasov, *Phys. Rev. B* **83**, 205101 (2011).
- [4] N. P. Armitage, E. J. Mele, and A. Vishwanath, *Rev. Mod. Phys.* **90**, 015001 (2018).
- [5] B. Q. Lv, H. M. Weng, B. B. Fu, X. P. Wang, H. Miao, J. Ma, P. Richard, X. C. Huang, L. X. Zhao, G. F. Chen, Z. Fang, X. Dai, T. Qian, and H. Ding, *Phys. Rev. X* **5**, 031013 (2015).
- [6] K.-Y. Yang, Y.-M. Lu, and Y. Ran, *Phys. Rev. B* **84**, 075129 (2011).
- [7] B. Q. Lv, N. Xu, H. M. Weng, J. Z. Ma, P. Richard, X. C. Huang, L. X. Zhao, G. F. Chen, C. E. Matt, F. Bisti, V. N. Strocov, J. Mesot, Z. Fang, X. Dai, T. Qian, M. Shi, and H. Ding, *Nat. Phys.* **11**, 724 (2015).
- [8] L. X. Yang, Z. K. Liu, Y. Sun, H. Peng, H. F. Yang, T. Zhang, B. Zhou, Y. Zhang, Y. F. Guo, M. Rahn, D. Prabhakaran, Z. Hussain, S.-K. Mo, C. Felser, B. Yan, and Y. L. Chen, *Nat. Phys.* **11**, 728 (2015).
- [9] A. A. Soluyanov, D. Gresch, Z. Wang, Q. Wu, M. Troyer, X. Dai, and B. A. Bernevig, *Nature (London)* **527**, 495 (2015).
- [10] L. Lu, L. Fu, J. D. Joannopoulos, and M. Soljačić, *Nat. Photonics* **7**, 294 (2013).
- [11] L. Lu, Z. Wang, D. Ye, L. Ran, L. Fu, J. D. Joannopoulos, and M. Soljačić, *Science* **349**, 622 (2015).
- [12] E. Goi, Z. Yue, B. P. Cumming, and M. Gu, *Laser Photonics Rev.* **12**, 1700271 (2018).
- [13] J. Noh, S. Huang, D. Leykam, Y. D. Chong, K. P. Chen, and M. C. Rechtsman, *Nat. Phys.* **13**, 611 (2017).
- [14] A. Cerjan, S. Huang, M. Wang, K. P. Chen, Y. Chong, and M. C. Rechtsman, *Nat. Photonics* **13**, 623 (2019).
- [15] Y. Lu, N. Jia, L. Su, C. Owens, G. Juzeliūnas, D. I. Schuster, and J. Simon, *Phys. Rev. B* **99**, 020302(R) (2019).
- [16] Y. Takahashi, T. Kariyado, and Y. Hatsugai, *Phys. Rev. B* **99**, 024102 (2019).
- [17] F. Li, X. Huang, J. Lu, J. Ma, and Z. Liu, *Nat. Phys.* **14**, 30 (2018).
- [18] X. Meng, W.-J. Chen, W.-Y. He, and C. T. Chan, *Nat. Phys.* **11**, 920 (2015).
- [19] M. Xiao, Q. Lin, and S. Fan, *Phys. Rev. Lett.* **117**, 057401 (2016).
- [20] W. Gao, B. Yang, M. Lawrence, F. Fang, B. Béni, and S. Zhang, *Nat. Commun.* **7**, 12435 (2016).
- [21] Q. Lin, M. Xiao, L. Yuan, and S. Fan, *Nat. Commun.* **7**, 13731 (2016).
- [22] C. Fang, M. J. Gilbert, X. Dai, and B. A. Bernevig, *Phys. Rev. Lett.* **108**, 266802 (2012).
- [23] M.-L. Chang, M. Xiao, W.-J. Chen, and C. T. Chan, *Phys. Rev. B* **95**, 125136 (2017).
- [24] S. Takahashi, S. Oono, S. Iwamoto, Y. Hatsugai, and Y. Arakawa, *J. Phys. Soc. Jpn.* **87**, 123401 (2018).
- [25] W.-J. Chen, M. Xiao, and C. T. Chan, *Nat. Commun.* **7**, 13038 (2016).
- [26] H. He, C. Qiu, X. Cai, M. Xiao, M. Ke, F. Zhang, and Z. Liu, *Nat. Commun.* **11**, 1820 (2020).
- [27] D. B. Fullager, G. D. Boreman, and T. Hofmann, *Opt. Mater. Express* **7**, 888 (2017).
- [28] S. G. Johnson and J. D. Joannopoulos, *Opt. Express* **8**, 173 (2001).
- [29] R. Resta, *J. Phys. Condens. Matter* **12**, R107 (2000).
- [30] See Supplemental Material at <http://link.aps.org/supplemental/10.1103/PhysRevLett.125.253902> for additional band structures, details on the Berry phase calculation, polarization analysis of Bloch modes and additional measurements at lower wavelengths.

- [31] G. von Freymann, A. Ledermann, M. Thiel, I. Staude, S. Essig, K. Busch, and M. Wegener, *Adv. Funct. Mater.* **20**, 1038 (2010).
- [32] T. Bückmann, N. Stenger, M. Kadic, J. Kaschke, A. Frölich, T. Kennerknecht, C. Eberl, M. Thiel, and M. Wegener, *Adv. Mater.* **24**, 2710 (2012).
- [33] I. Staude, M. Thiel, S. Essig, C. Wolff, K. Busch, G. von Freymann, and M. Wegener, *Opt. Lett.* **35**, 1094 (2010).
- [34] V. Liu and S. Fan, *Comput. Phys. Commun.* **183**, 2233 (2012).
- [35] T.-H. Kao, L.-Y. C. Chien, and Y.-C. Hung, *Opt. Express* **23**, 24416 (2015).
- [36] I. Karakasoglu, M. Xiao, and S. Fan, *Opt. Express* **26**, 21664 (2018).
- [37] M. Saba, M. Thiel, M. D. Turner, S. T. Hyde, M. Gu, K. Grosse-Brauckmann, D. N. Neshev, K. Mecke, and G. E. Schröder-Turk, *Phys. Rev. Lett.* **106**, 103902 (2011).
- [38] S. Takahashi, T. Tajiri, Y. Ota, J. Tatebayashi, S. Iwamoto, and Y. Arakawa, *Appl. Phys. Lett.* **105**, 051107 (2014).
- [39] X. Wan, A. M. Turner, A. Vishwanath, and S. Y. Savrasov, *Phys. Rev. B* **83**, 205101 (2011).
- [40] A. F. Oskooi, D. Roundy, M. Ibanescu, P. Bermel, J. Joannopoulos, and S. G. Johnson, *Comput. Phys. Commun.* **181**, 687 (2010).